

Molecular Insight from DFT Computations and Kinetic Measurements into the Steric Factors Influencing Peptide Bond Hydrolysis Catalyzed by a Dimeric Zr(IV)-Substituted Keggin Type Polyoxometalate

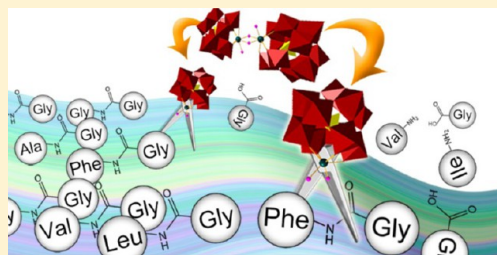
Tzvetan T. Mihaylov,^{*,†} Hong Giang T. Ly,[‡] Kristine Pierloot,[†] and Tatjana N. Parac-Vogt[‡]

[†]Laboratory of Computational Coordination Chemistry, Department of Chemistry, KU Leuven, Celestijnenlaan 200F, 3001 Leuven, Belgium

[‡]Laboratory of Bioinorganic Chemistry, Department of Chemistry, KU Leuven, Celestijnenlaan 200F, 3001 Leuven, Belgium

Supporting Information

ABSTRACT: Peptide bond hydrolysis of several peptides with a Gly-X sequence (X = Gly, Ala, Val, Leu, Ile, Phe) catalyzed by a dimeric Zr(IV)-substituted Keggin type polyoxometalate (POM), $(\text{Et}_2\text{NH}_2)_8[\{\alpha\text{-PW}_{11}\text{O}_{39}\text{Zr}(\mu\text{-OH})(\text{H}_2\text{O})\}_2]\cdot 7\text{H}_2\text{O}$ (**1**), was studied by means of kinetic experiments and ^1H NMR spectroscopy. The observed rate of peptide bond hydrolysis was found to decrease with increase of the side chain bulkiness, from $4.44 \times 10^{-7} \text{ s}^{-1}$ for Gly-Gly to $0.81 \times 10^{-7} \text{ s}^{-1}$ for Gly-Ile. A thorough DFT investigation was performed to elucidate (a) the nature of the hydrolytically active species in solution, (b) the mechanism of peptide bond hydrolysis, and (c) the influence of the aliphatic residues on the rate of hydrolysis. Formation of substrate–catalyst complexes of the dimeric POM **1** was predicted as thermodynamically unlikely. Instead, the substrates prefer to bind to the monomerization product of **1**, $[\alpha\text{-PW}_{11}\text{O}_{39}\text{Zr}(\text{OH})(\text{H}_2\text{O})]^{4-}$ (**2**), which is also present in solution. In the hydrolytically active complex two dipeptide ligands are coordinated to the Zr(IV) center of **2**. The first ligand is bidentate-bound through its amino nitrogen and amide oxygen atoms, while the second ligand is monodentate-bound through a carboxylic oxygen atom. The mechanism of hydrolysis involves nucleophilic attack by a solvent water molecule on the amide carbon atom of the bidentate-bound ligand. In this process the uncoordinated carboxylic group of the same ligand acts as a general base to abstract a proton from the attacking water molecule. The decrease of the hydrolysis rate with an increase in the side chain bulkiness is mostly due to the increased ligand conformational strain in the rate-limiting transition state, which elevates the reaction activation energy. The conformational strain increases first upon substitution of H_α in Gly-Gly with the aliphatic α substituent and second with the β branching of the α substituent.



INTRODUCTION

Selective hydrolysis of peptide bonds in proteins plays an important role in a broad range of research fields such as chemical biology, proteomics, and drug discovery.¹ The reaction is also frequently applied in structural determinations of peptides and proteins. Proteolytic enzymes with a high catalytic power can be used for this purpose. However, they often operate only in a narrow range of temperature and pH. In addition, the high cost and limited or fixed selectivity of proteolytic enzymes has led to the search for alternative cleavage agents for hydrolysis of peptide bonds, which are extremely stable at physiological pH and room temperature.²

Polyoxometalates (POMs) are generally described as clusters of early-transition-metal ions in their highest oxidation state bridged by oxo anions. Owing to their fascinating properties such as tunable acidity and redox properties, high thermal stability, hydrolytic and oxidative stability, POMs have been applied in broad fields including catalysis,³ materials,⁴ and medicine.⁵ In recent years applications of POMs for catalytic purposes have also been extensively investigated. Series of

reviews and publications focusing on the use of POMs in heterogeneous catalysis,⁶ electrocatalysis,⁷ water oxidation,⁸ and oxidation of organic compounds⁹ have been published. In order to improve or tune the catalytic properties of POMs, lanthanide or transition-metal ions can be introduced into the skeleton of vacant POMs to form metal-substituted POMs (MSPs). The combination of the POM framework, with its negative charge playing a role in electrostatic interaction with positively charged substrates, and the active metal sites, which can coordinate water or other ligands at their free coordination sites, makes such MSPs attractive for catalytic applications. In addition, the introduction of metal ions into the POM framework can stabilize them, preventing gel formation in aqueous solution.¹⁰ The first investigations concerned the catalytic properties of Ti(IV)- and Zr(IV)-substituted POMs toward oxidation reactions with H_2O_2 .¹¹ The use of MSPs as catalysts for a broad range of chemical reactions, such as H_2O_2 -based

Received: June 17, 2016

oxidation of organic compounds,¹² cyclization of citronellal derivatives,¹³ Diels–Alder reactions and aldol reactions of imines,¹⁴ oxygenation of catechols,¹⁵ synthesis of cyclic carbonates,¹⁶ oximation of aldehydes and ketones,¹⁷ and the splitting of water,¹⁸ has recently been reported.

In our quest to develop MSPs as potential catalysts for peptide bond hydrolysis, Zr(IV)- and Ce(IV)-substituted POMs have been used, because both Zr(IV) and Ce(IV) have a high Lewis acidity, oxophilicity, and kinetic lability and tend to form complexes with high coordination numbers. The hydrolytic activity of a series of Zr(IV)-substituted Keggin, Lindqvist, and Wells–Dawson POMs toward peptide bond hydrolysis in dipeptides^{10a,b,19} and oligopeptides²⁰ was discovered previously. All complexes act as homogeneous catalysts and significantly accelerate the hydrolysis reaction rates in mildly acidic and neutral pH environments. In addition, we recently showed that a Ce(IV)-substituted Keggin POM and Zr(IV)-substituted Keggin, Lindqvist, and Wells–Dawson POMs selectively hydrolyze proteins such as hen egg white lysozyme, albumins, and horse heart myoglobin, thus demonstrating the potential of Ce(IV)- and Zr(IV)-substituted POMs as novel artificial proteases.^{10c,21}

In aqueous solution, dimeric Zr(IV)-substituted POMs can partially dissociate into monomeric species, which are presumed to be the active species during the catalytic reactions.^{10b,19a} For example, the 1:1 Zr(IV)-Keggin POM $[\alpha\text{-PW}_{11}\text{O}_{39}\text{Zr}(\text{OH})(\text{H}_2\text{O})]^{4-}$ was identified as the active compound for the hydrolysis of DNA-model phosphoesters by both experimental and theoretical means,²² even though the dimeric 2:2 Zr(IV)-Keggin POM $[\{\alpha\text{-PW}_{11}\text{O}_{39}\text{Zr}(\mu\text{-OH})(\text{H}_2\text{O})\}_2]^{8-}$ (**1**) was used as a starting catalyst (see Figure 1).²² This may be the reason for the superior hydrolytic activity of **1** toward myoglobin, in comparison to other POMs which do not undergo dissociation.^{10c,23}

The selectivity of **1** toward dipeptides containing different amino acid sequences (other than those studied here) was recently reported, and the results indicated that the reaction

rate is dependent on the nature and the bulkiness of the amino acid side chain.^{19c} The first mechanistic study on peptide bond hydrolysis catalyzed by a dimeric tetrazirconium(IV) Wells–Dawson POM was also reported recently by us.²³ For dipeptides with aliphatic residues the hydrolytically active substrate–catalyst complex is formed through bidentate chelate coordination of the ligand to a Zr(IV) center of the POM, involving the amino nitrogen and the amide oxygen atoms, while the terminal ligand carboxylic group remains uncoordinated. In the rate-determining reaction step the latter acts as a general base to facilitate nucleophilic attack by a solvent water molecule on the amide carbon atom. Similar to the case for **1**, the rates of hydrolysis within a series of dipeptides were also found with this catalyst to be dependent on both the nature and the bulkiness of the side chains. The molecular factors governing this selectivity, however, remain unclear. The large variety of amino acid sequences involved in the dipeptide series presupposes a variety of different substrate–catalyst complexes and possible mechanistic scenarios for hydrolysis. For instance, some of the dipeptides involve amino acids with residues that could coordinate to Zr(IV), such as Gly–Asn, Gly–Asp, Gly–Gln, Gly–His, Gly–Ser, and Gly–Thr, while others with positively charged residues, such as Gly–Lys and Gly–Arg, may stabilize the complex through electrostatic interactions with the negatively charged POM surface. Therefore, the coordination behavior and the mechanisms of hydrolysis should be clarified individually in every particular case.

This study is focused on the hydrolytic activity of **1** toward a series of dipeptides with a common Gly–X sequence, where X is an amino acid with an aliphatic (noncoordinating) side chain, such as Ala, Val, Leu, Ile, and Phe. In this series both the coordination behavior and the mechanisms of hydrolysis are expected to be rather similar, which allows us to distinguish the role of the aliphatic side chain in the process. However, the tendency of the parent compound **1** for partial dissociation in solution brings additional complexity to the problem studied. The kinetics of the Gly–X dipeptide hydrolysis in the presence of **1** was studied experimentally by an ¹H NMR method. To explain the experimental findings, the nature of the hydrolytically active species, the mechanism of peptide bond hydrolysis, and the effect of the aliphatic residues on the rate of hydrolysis were investigated on a molecular level by means of density functional methods.

EXPERIMENTAL SECTION

Chemicals. $(\text{Et}_2\text{NH}_2)_8[\{\alpha\text{-PW}_{11}\text{O}_{39}\text{Zr}(\mu\text{-OH})(\text{H}_2\text{O})\}_2]\cdot 7\text{H}_2\text{O}$ (**1**) was synthesized according to the procedure given in the literature.^{10b,24} D_2O , DCl, NaOD, $\text{H}_3\text{PW}_{12}\text{O}_{40}\cdot 23\text{H}_2\text{O}$, and the dipeptides used in this study were purchased from Sigma-Aldrich.

NMR Measurements. ¹H NMR spectra were recorded on a Bruker Advance 400 spectrometer, and TMS-*d*₄ was used as an internal reference.

Hydrolysis Studies. The hydrolysis reaction mixtures typically contain 2.0 mM dipeptide, 2.0 mM **1**, and 0.5 mM TMS-*d*₄ (sodium 3-trimethylsilylpropionate) in D_2O . The pD of the reaction mixtures was adjusted to 5.4 with minor amounts of 1.0 M DCl or 1.0 M NaOD. The pH-meter reading was corrected by the equation $\text{pD} = \text{pH} + 0.41$.²⁵ The reaction mixtures were kept at 60 °C, and ¹H NMR spectra were taken after mixing and after different time increments. The hydrolysis products were identified by comparison of the ¹H NMR chemical shifts with those of the pure amino acids at the same pD value. The rate constants (k_{obs}) were calculated by fitting the decrease in dipeptide concentration to a first-order monoexponential decay function.

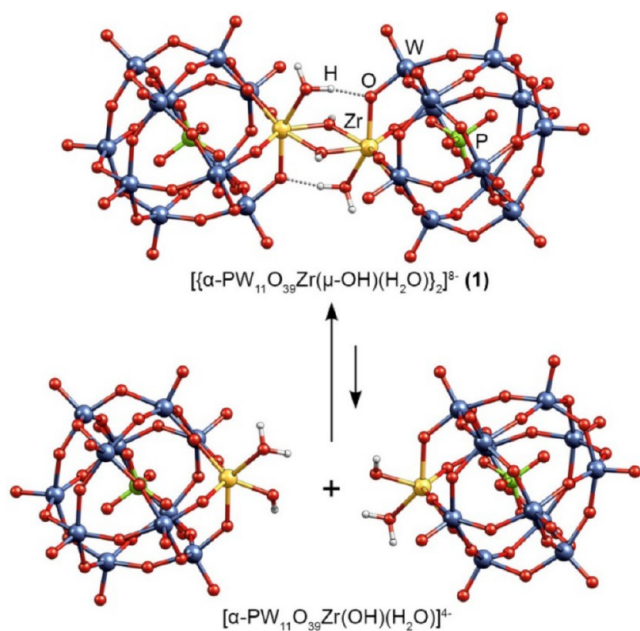
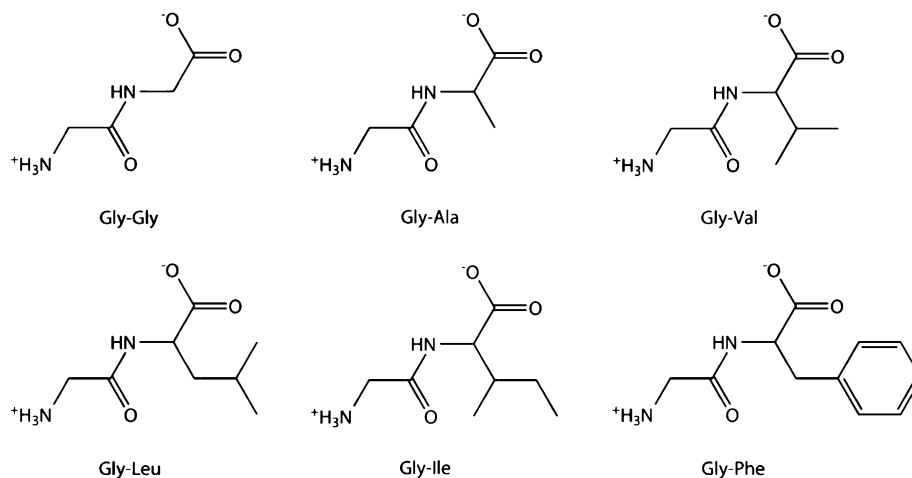


Figure 1. Molecular structures of 2:2 Zr(IV)-Keggin and 1:1 Zr(IV)-Keggin POMs.

Scheme 1. Structures of Gly-X Dipeptides



Computational Methods. Binding Study. DFT calculations were performed with the ORCA program package,²⁶ version 3.0. Molecular geometries were fully optimized (without symmetry constraints) employing the gradient-corrected BP86²⁷ functional and def2-SVP basis sets.²⁸ MWB28 and MWB60 Stuttgart–Dresden effective core potentials²⁹ (ECPs) were used to replace the core electrons of Zr and W atoms, respectively. To speed up the calculations, the Split-RI-J variant³⁰ of the resolution of the identity (RI) technique³¹ with auxiliary def2-SVP/J Coulomb fitting basis sets³² was employed (applying an increased integration grid, Grid4 in the ORCA convention, and tight SCF convergence criteria). The effects of the aqueous solvent were included in the geometry optimizations by using the conductor-like screening model (COSMO),³³ as implemented in ORCA. The BP86 functional has already been used for geometry optimization of various POMs in a number of theoretical works.³⁴ A comparison of the structural parameters for $[\{\alpha\text{-PW}_{11}\text{O}_{39}\text{Zr}(\mu\text{-OH})(\text{H}_2\text{O})\}_2]^{8-}$ (**1**) obtained in this study and those determined by X-ray analysis of $(\text{Et}_2\text{NH}_2)_8[\{\alpha\text{-PW}_{11}\text{O}_{39}\text{Zr}(\mu\text{-OH})(\text{H}_2\text{O})\}_2]\cdot 7\text{H}_2\text{O}$ ^{24b} in general showed a good agreement. Selected theoretical vs experimental structural parameters may be found in Table S1 of the Supporting Information. To find the lowest energy structures, a conformational search was performed for all species under consideration (except **1**, for which the X-ray structure was used as the input geometry). To verify that the stationary points found are minima on the potential energy surface (PES) and to obtain the thermochemical data, numerical vibrational frequencies were computed using the standard rigid rotor-harmonic oscillator approximation. In order to refine the energies, single-point (SP) calculations on the BP86 optimized structures were performed by means of the hybrid density functional B3LYP³⁵ and more extended basis sets, def2-TZVP,²⁸ combined with the COSMO model. For the Zr and W atoms the aforementioned ECPs were still used. The Split-RI-J combined with the chain of spheres approximation to the exact exchange (RIJCOSX)³⁶ was utilized with the auxiliary def2-TZVP/J Coulomb fitting basis sets³² (applying Grid5, GridX5, and tight SCF convergence criteria). When it is applied with the B3LYP functional, the RIJCOSX approximation is expected to introduce a negligible error in the reaction energies in comparison to the approximation free calculations.³⁶ To account for dispersion forces, missed in the pure B3LYP method, Grimme's atom-pairwise dispersion correction with Becke–Johnson damping (D3BJ)³⁷ was employed.

A detailed description of the strategy used for estimation of the free energies of complexation is given in the Computational Details section of the Supporting Information.

Reaction Path Modeling. This part of the calculations was performed with the Gaussian 09 Rev. D.01 suite of programs.³⁸ Geometry optimizations and frequency calculations were performed with the hybrid meta-GGA functional M06-2X³⁹ and 6-31+G(d,p) basis sets; for the Zr and W atoms LANL2DZ⁴⁰ ECPs/basis sets were

applied. Due to the large size of the transition state (TS) complexes, intrinsic reaction coordinate (IRC) calculations were performed only in a few cases where we had doubts about the nature of the TS obtained. Otherwise, the TS structures were judged by analyzing the atomic movements of the corresponding imaginary frequencies. The bulk solvent effects were included in the geometry optimizations by means of the CPCM⁴¹ solvation model with the default parameters (UFF cavities). However, the final free energies of solvation were obtained with Pauling atomic radii, taking into account the nonelectrostatic energy contributions. The electronic energies of the stationary points were adjusted in SP calculations utilizing the M06-2X-D3, M06-D3,³⁹ and BMK-D3⁴² functionals (D3 means that the original D3 damping function^{37b} is used instead of the BJ function) with def2-TZVP basis sets and MWB28/MWB60 ECPs for the Zr/W atoms. These functionals were selected on the basis of our previous study on POM-catalyzed peptide bond hydrolysis.²³

A standard state of 1 mol L⁻¹ was used for all compounds except water molecules, for which a 55.34 mol L⁻¹ standard state was used instead.⁴³

RESULTS AND DISCUSSION

Hydrolysis of Gly-X Peptides. The hydrolysis of a series of Gly-X peptides in which X = Gly, Ala, Val, Leu, Ile, Phe (Scheme 1) in the presence of **1** was examined in solution containing equimolar amounts (2.0 mM) of the dipeptide and **1** at pD 5.4 and 60 °C. ¹H NMR spectra of the hydrolysis reactions were recorded at different reaction times, and the hydrolysis product glycine (Gly) was identified by a singlet peak at 3.57 ppm^{10b} (Figures S1–S6 of the Supporting Information). The amounts of the reacted dipeptide and of the free Gly were determined by integration of their respective ¹H NMR resonances, and the rate constants (k_{obs}) were calculated by fitting the decrease in dipeptide concentration to a monoexponential decay function. The hydrolysis of all studied dipeptides in the absence of **1** under the same experimental conditions was also studied as a control reaction. Fully homogeneous solutions were observed during the hydrolytic reaction of all dipeptides, indicating that the presence of dipeptides does not affect the stability of **1**.^{10b,19c}

The values of calculated rate constants for Gly-X hydrolysis are collected in Table 1. Due to the extreme stability of the peptide bond in the absence of **1**, the rate constants for the uncatalyzed hydrolysis of dipeptides could not be determined under these conditions. However, the amount of dipeptide hydrolyzed in the absence of **1** after 7 months could be

Table 1. Observed Rate Constants for the Hydrolysis of Gly-X in the Absence and Presence of **1**^a

peptide	conversion after 7 months (%) (without 1)	$10^7 k_{\text{obs}}$ (s^{-1}) (with 1)
Gly-Gly	25	4.44 ± 0.10
Gly-Ala	5	3.89 ± 0.37
Gly-Val	0	1.71 ± 0.19
Gly-Leu	0	1.72 ± 0.35
Gly-Ile	0	0.81 ± 0.11
Gly-Phe	0	2.53 ± 0.15

^aConditions: $[1] = [\text{dipeptide}] = 2.0 \text{ mM}$, pD 5.4, 60 °C.

estimated and is also shown in Table 1. From these results it is clear that all dipeptides are very stable and that their hydrolysis was significantly accelerated by **1**. The mechanism of Gly-Gly hydrolysis in the presence of Zr-POMs was previously suggested to occur via coordination of Gly-Gly to a Zr(IV) ion via its amide oxygen and amine nitrogen atoms.^{10b,23} This interaction results in polarization of the amide C=O bond, making it more susceptible toward nucleophilic attack by a water molecule.

The dependence of the hydrolysis rate constants on the volume of the amino acid side chain⁴⁴ at the C terminus is shown in Figure 2. From this figure it can be seen that the

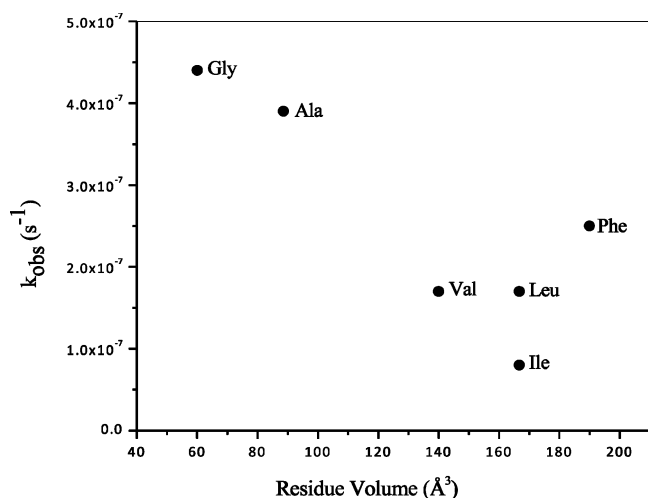


Figure 2. Reaction rate constants for the hydrolysis of 2.0 mM Gly-X dipeptides in the presence of 2.0 mM **1** at pD 5.4 and 60 °C as a function of the volume of amino acid X.

hydrolysis rate constant decreases when the volume of the noncoordinating X amino acid side chain is increased, implying that steric hindrance either impairs the interaction between the Zr(IV) ion and the dipeptide or prevents efficient nucleophilic attack of water or hydroxide. Interestingly, despite its higher molecular volume in comparison to that of Gly-Val, Gly-Ile, and Gly-Leu, a higher rate constant was obtained for Gly-Phe.

To shed light on the hydrolytic processes at the atomistic level, we have first studied the coordination properties of the Gly-X dipeptides to the Zr(IV) atom(s) of the POM in order to discern the potential hydrolytically active species in solution. In a second step, the most likely candidates were used to model possible reaction paths of hydrolysis. Since in the series Gly-X the substrates differ only in their aliphatic (noncoordinating) residues, we can safely assume that their coordination properties will be rather similar. Thus, for the purpose of the

binding study, we have performed a DFT investigation on the coordination behavior of the simplest dipeptide of this series, Gly-Gly.

Coordination Properties of Gly-Gly toward Zr(IV)-Substituted Keggin POMs. *Coordination of Gly-Gly to 2:2 Zr(IV)-Keggin POM (1).* There are four different basic sites in the Gly-Gly zwitterion suitable for coordination to Zr(IV): the terminal amino nitrogen, the terminal carboxylic oxygens, the amide oxygen, and the amide nitrogen. As previously demonstrated for Cu(I), Ni(I), and Co(I) ions, tri- and bidentate modes of Gly-Gly coordination are much more plausible than monodentate coordination modes. In addition, the most plausible binding mode varies depending on the metal ion and is either bidentate (for Cu(I)), through the terminal amino and carboxylic groups, or tridentate (for Ni(I) and Co(I)), involving in addition the amide nitrogen or oxygen atom.⁴⁵ It should be noted that in the case of **1** tridentate binding to one metal center would result in a 9-coordinated zirconium, which is unlikely, as the coordination number typical of Zr(IV) complexes including POMs is 7 or 8.⁴⁶ Due to steric hindrance caused by the bulky Keggin POM ligands, our attempts to model even bidentate coordination of Gly-Gly to one Zr atom of **1** were unsuccessful. Therefore, the most feasible bidentate modes of coordination were constructed, where the dipeptide bridges the two neighboring Zr atoms, by varying the basic sites of Gly-Gly interacting with the metals. The optimized molecular structures, the free energies of complexation, and their discussion can be found in Figure S7, Table S2, and the Coordination of Gly-Gly to Compound **1** section in the Supporting Information, respectively. In all cases positive free energies of complexation, in the range of 0.7–18.5 kcal mol⁻¹, were computed. Thus, our DFT calculations predict that the formation of a complex between Gly-Gly and **1** is thermodynamically unfavorable. Only in the case of bidentate bridging coordination through the terminal carboxylic group was a free energy of complexation close to 0 obtained (0.7 kcal mol⁻¹), indicating that such a complex may occur in the reaction mixture. This result, however, cannot explain the hydrolytic activity of **1**. Moreover, the ¹³C NMR data showed no evidence for –COO⁻ binding but instead suggest metal–ligand interaction involving the terminal amino and peptide carbonyl groups.^{10b} According to the calculations, however, formation of such a complex with **1** is rather unlikely, as this requires ~12 kcal mol⁻¹ (at near neutral pH).

These results have stimulated us to find another explanation for the hydrolytic activity of **1**.

Coordination of Gly-Gly to 1:1 Zr(IV)-Keggin POM (2). Depending on the pH, temperature, time, concentration, and the presence of ligands, the parent compound **1** may undergo partial dissociation in aqueous solution leading to the formation of both 1:2 species $[\text{Zr}(\alpha\text{-PW}_{11}\text{O}_{39})_2]^{10-}$ with the lacunary anion $[\alpha\text{-PW}_{11}\text{O}_{39}]^{7-}$ and of monomeric species $[\alpha\text{-PW}_{11}\text{O}_{39}\text{Zr}(\text{OH})_n(\text{H}_2\text{O})_{3-n}]^{(3+n)-}$ ($n = 0, 1$).^{11c,26b} The 1:2 complex appears in basic solution and shows a very low reactivity toward peptide bond hydrolysis,^{10b} most probably because of the lack of free coordination sites at the Zr(IV) center when it is sandwiched between the two Keggin moieties. Therefore, substrate coordination to the 1:2 complex was not examined in our DFT models. The presence of monomeric species has first been suggested on the basis of ³¹P NMR signals under strongly acidic conditions (0.1 M aqueous HCl) by Nomiyama et al.^{24b} and in MeCN solution by Kholdeeva et al.^{11c} Recently, Jiménez-Lozano et al. have calculated the energy of

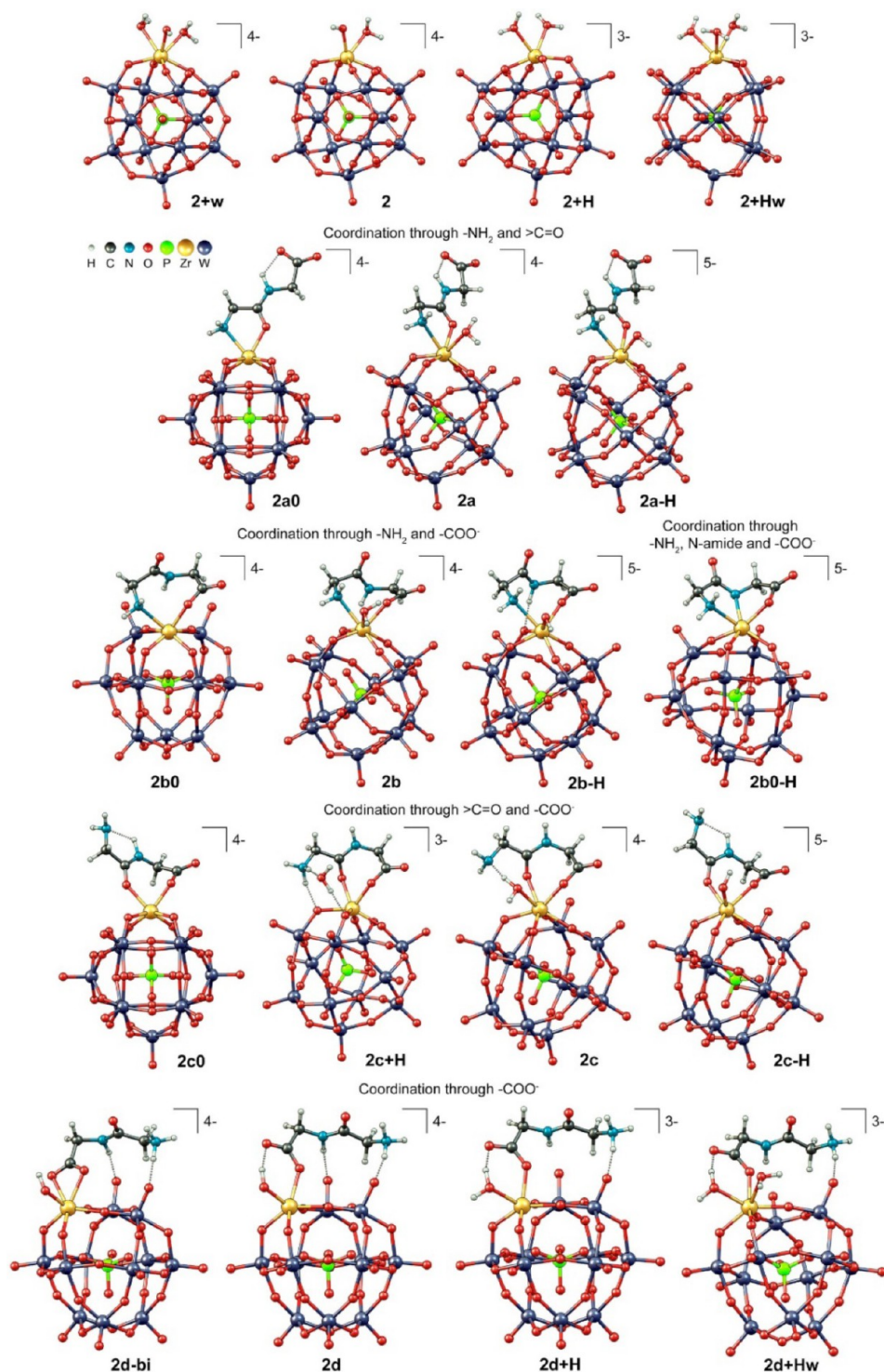


Figure 3. DFT optimized structures of the Gly-Gly complexes with **2**.

the reaction $2[\text{PW}_{11}\text{O}_{39}\text{Zr}(\text{OH})(\text{H}_2\text{O})]^{4-} \rightarrow \{[\alpha\text{-PW}_{11}\text{O}_{39}\text{Zr}(\mu\text{-OH})(\text{H}_2\text{O})]_2\}^{8-}$. With use of PCM-B3LYP (with double- ζ basis sets and LANL2DZ ECPs for W and Zr) a dimerization energy of $-23.6 \text{ kcal mol}^{-1}$ was obtained.⁴⁷ However, in terms of the free energy in the aqueous phase, ΔG_{aq}^* , this dimerization energy is reduced to $-3.4 \text{ kcal mol}^{-1}$, suggesting that the monomeric species coexists in equilibrium with **1**.²² Finally, the presence of the monomer in solution at pH 6.4 was confirmed by means of ^{31}P NMR and ^{31}P DOSY experiments.²² Even when it is present in minor concentrations, the monomer

could play a major role in the hydrolytic process. Indeed, formation of a stable monomer–substrate complex may shift the equilibrium in favor of the monomer.⁴⁸

To further investigate this, the coordination behavior and binding energy of Gly-Gly at the monomeric species were investigated more closely. First, the most stable monomeric form with respect to the coordination number and protonation state of H_2O molecules to Zr was identified. In order to judge whether a $\text{Zr}\text{-OH}_2$ is deprotonated or not at the environmental pH the $\text{p}K_{\text{a}}$ value of a H_2O ligand was estimated (by

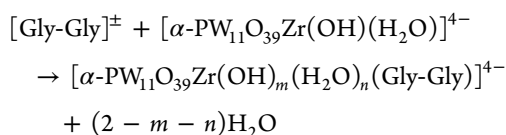
Table 2. Formation Free Energy (kcal mol⁻¹) of the Coordination Compounds of Gly-Gly and 2

species ^a	$\Delta G_{\text{aq}}^{\text{compl}}$	$\text{p}K_{\text{a}}/\text{p}K_{\text{b}}$	$\Delta G^{\text{deprot/prot}}$	species ^b	$\Delta G_{\text{aq}}^{\text{compl}}(\text{pH})$
2a0	-1.1 (1.2) ^c				
2a	-0.9 (1.6)	3.8	-3.6	→2a-H	-4.5 (-5.6)
2b0	-5.2 (-7.0)	11.3 (>NH)	6.7 (>NH)	→2b0-H	1.6 (0.2)
2b	-4.2 (-5.0)	10.0	5.0	→2b-H	0.8 (1.8)
2c0	-2.5 (-1.6)				
2c	-1.9 (-0.4)	7.0 (NH ₂)	-0.8 (-NH ₂)	→2c+H	-2.8 (-2.2)
		11.1	6.4	→2c-H	4.4 (12.2)
2d	-1.9 (-0.4)				
2d-bi	-2.5 (-1.6)	3.7	-5.4	→2d+H	-7.9 (-12.4)
				2d+Hw	-6.8 (-10.2)

^aCoordination compounds formed according to the reaction given in the text (for more details see the [Computational Details](#) section in the Supporting Information). ^bSpecies obtained via deprotonation/protonation of the corresponding compounds in the first column (for more details see the [Computational Details](#) section in the Supporting Information). ^cEnergy values in parentheses are relative to the parent compound 1, assuming that both generated monomeric species 2 react with Gly-Gly ligands.

applying eq 9 in the [Computational Details](#) section of the Supporting Information) for the structure 2+H, shown in [Figure 3](#). It should be noted that the accurate estimation of $\text{p}K_{\text{a}}$ values of highly charged species, such as POMs, is a challenging task by itself, implying more complicated thermodynamic cycles and approaches.⁴⁹ Nevertheless, the approach used here seems sufficiently reliable for the purpose of this study, as the calculated $\text{p}K_{\text{a}} = 0.6$ is in good agreement with reported data for a Zr(IV)-bound water molecule ($\text{p}K_{\text{a}} \leq 0.6$).⁵⁰ Such a $\text{p}K_{\text{a}}$ value enables the deprotonated form 2 to readily exist in neutral media. Coordination of an additional water molecule, giving rise to structures 2+Hw and 2+w in [Figure 3](#), is found to be slightly endergonic for both 2+H and 2, by 1.4 and 1.7 kcal mol⁻¹, respectively. Therefore, structure 2 was used to obtain the free energy change upon coordination of Gly-Gly[±] to the monomeric Zr-POM.

As was done for structure 1, many possible Gly-Gly complexes of 2 in their different protonation states were modeled. Only the lowest energy conformations are depicted in [Figure 3](#). Note that, with the exception of structure 2b0-H (where the amide N is deprotonated and acts as the third ligand), either mono- or bidentate Gly-Gly coordination is obtained for all structures. The free energies of complexation ($\Delta G_{\text{aq}}^{\text{compl}}$) were calculated according to the reaction



where, depending on the ligand binding mode, m can be either 0 (where the Zr-OH ligand has received a proton from the substrate -NH₃⁺ group) or 1. For $m = 0$, $n = 0-2$, while for $m = 1$, $n = 0, 1$. Energy data are summarized in [Table 2](#). The species shown in the left-hand column of [Table 2](#) are formed through the reaction above, whereas the structures at the right-hand side are obtained after deprotonation/protonation of the original reaction products. The formation free energies of the latter were obtained by adjusting the corresponding $\Delta G_{\text{aq}}^{\text{compl}}$ values with the free energy change due to deprotonation/protonation at the environmental pH, $\Delta G_{\text{aq}}^{\text{compl}}(\text{pH}) = \Delta G_{\text{aq}}^{\text{compl}} + \Delta G^{\text{deprot/prot}}$. More details can be found in the [Computational Details](#) section of the Supporting Information. The pH value of 6.4 was chosen for the binding studies to enable comparison of the theoretical results with the suggested coordination mode of Gly-Gly to the POM on the basis of ¹³C

NMR measurements (previously performed by us) at this pH.^{10b} Coordination in the species labeled a occurs through the terminal amino and peptide carbonyl groups, in species b through the terminal amino and carboxyl groups, and in species c through the carbonyl and carboxyl groups. In the three species 2a-c, Gly-Gly is coordinated as an anion. These structures are obtained from 2 by protonation of Zr-OH by the ligand -NH₃⁺ group and simultaneous ligand exchange (water release). In structures 2a0-c0 the remaining H₂O is also dissociated. As can be seen from [Table 2](#), all three types of Gly-Gly coordination are found to be exergonic, releasing an energy of between 0.9 and 5.2 kcal mol⁻¹. In the species labeled d, Gly-Gly coordination involves only the substrate -COO⁻ group, either mono- (2d) or bidentate (2d-bi). Here, Gly-Gly is coordinated as a zwitterion and has replaced a water ligand in structure 2. Bidentate coordination is only slightly more stable than monodentate coordination, by 0.6 kcal mol⁻¹, and both structures are similar in energy to the alternative coordination modes a-c.

As all three species 2a-c contain a H₂O ligand, deprotonation of this ligand might be favorable, giving rise to the species 2a-H-c-H. The corresponding $\text{p}K_{\text{a}}$ values were found to be 3.8, 10.0, and 11.1. This means that further stabilization by deprotonation is only expected for species 2a, with a calculated energy gain (at pH 6.4) of -3.6 kcal mol⁻¹, giving rise to a net formation energy ($\Delta G_{\text{aq}}^{\text{compl}}(\text{pH})$) of -4.5 kcal mol⁻¹ for complex 2a-H. On the other hand, species 2d and 2d-bi contain an -OH ligand. The basicity of this -OH was also estimated. Starting from the most stable 2d-bi structure, a $\text{p}K_{\text{b}}$ value of 3.7 was calculated, corresponding to a gain in free energy of 5.4 kcal mol⁻¹ for protonation (at pH 6.4). Note that protonation gives rise to a complex with a monocoordinated carboxylate group, 2d+H. The corresponding bidentate structure was found to be less stable by 5 kcal mol⁻¹ and is not included in [Figure 3](#). Coordination of a second water molecule to 2d+H does not lead to additional stabilization of this complex (structure 2d+Hw).

Finally, two other acid-base reactions were found to give rise to structures with energies similar to those already considered. The first is structure 2b0-H, obtained from deprotonation of the amide nitrogen in 2b0. As [Figure 3](#) shows, 2b0-H is a tridentate complex. However, its formation from 2b0 is endergonic by 6.7 kcal mol⁻¹ ($\text{p}K_{\text{a}} = 11.3$). The second structure is 2c+H, obtained from 2c by protonation of the ligand -NH₂ group. With a $\text{p}K_{\text{b}}$ of 7.0, protonation is slightly

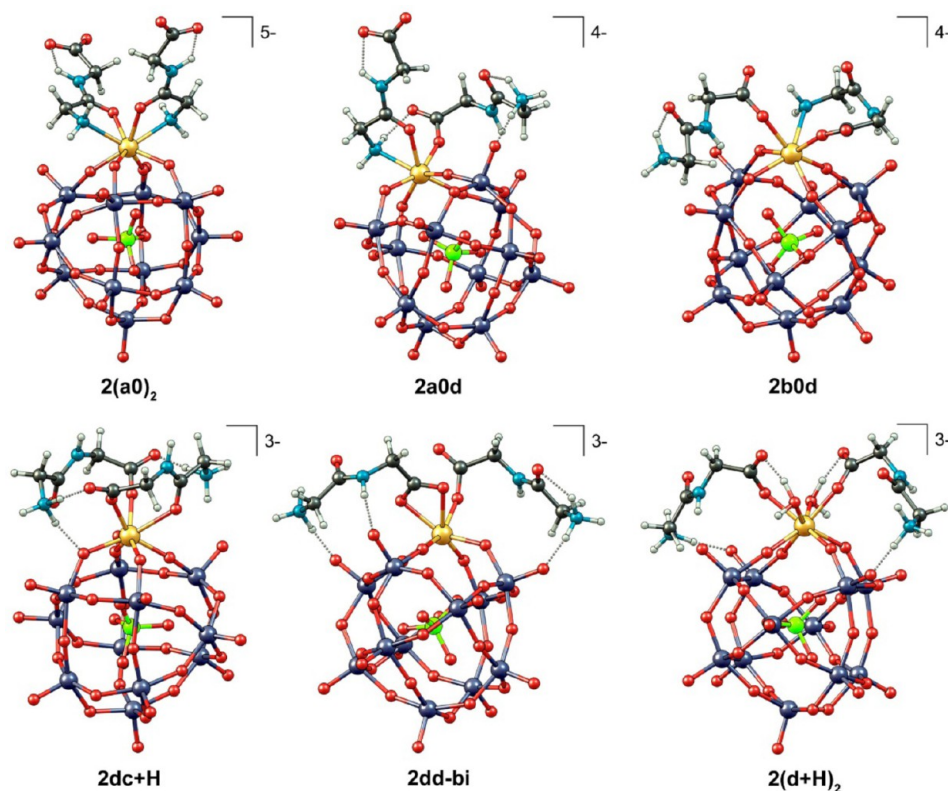


Figure 4. DFT optimized structures with two Gly-Gly ligands coordinated to **2**.

avored, by $0.8 \text{ kcal mol}^{-1}$, at pH 6.4. However, one can observe that in structure **2c+H** the Zr–OH₂ bond is broken, and a HO–H···O–Zr H bond is formed instead.

In order to compare the results obtained for **2** with those for the initial compound **1** (Table S2 of the Supporting Information), the free energy change corresponding to the net reaction (dimer) + 2 GlyGly → 2(monomer complex) should be used. These values are provided in parentheses in Table 2. Even though these formation energies must be considered more or less qualitatively (e.g., an error of 1 pK_a value introduces an error of $1.4 \text{ kcal mol}^{-1}$ in the $\Delta G_{\text{aq}}^{\text{compl}}(\text{pH})$ value), our calculations undoubtedly show that substrate coordination to the monomeric POM is largely preferred in comparison to the initial dimer.

1:1 Zr(IV)-Keggin POM Complexes with Two Gly-Gly Ligands. In the case of **2** coordination of a second Gly-Gly ligand to the Zr(IV) center is also possible. To examine this scenario, a series of complexes were modeled by testing different binding modes of Gly-Gly to the **2a0**, **2b0**, **2c+H**, and **2d+H** species. These species were selected on the basis of their stability, for every particular binding mode, and the availability of free coordination sites at the Zr(IV) center (six-coordinated zirconium ion). The resultant optimized structures and their formation energies are given in Figure 4 and Table 3 respectively. With the exception of **2b0d** and **2(d+H)₂**, the addition of a second Gly-Gly ligand to structures **2a0**, **2b0**, **2c+H**, and **2d+H** (with or without H₂O release) was found to be exergonic by $0.4 \text{ kcal mol}^{-1}$ (**2dd-bi**) to 8.0 (**2a0d**) kcal mol^{-1} . However, comparison of the formation free energies in Tables 2 and 3 reveals that there is no substantial stabilization effect upon coordination of a second substrate molecule to **2** instead of a H₂O/OH ligand. Thus, the calculations predicted that in the reaction mixture Gly-Gly complexes with **2** involving either

Table 3. Formation Free Energy (kcal mol^{-1}) of the Complexes Obtained through Coordination of Two Gly-Gly Ligands to **2**

species	$\Delta G_{\text{aq}}^{\text{compl}}/\Delta G_{\text{aq}}^{\text{compl}}(\text{pH})$
2(a0)₂	−3.6 (−3.9) ^a
2a0d	−9.1 (−14.8)
2b0d	−1.3 (0.7)
2dc+H	−7.6 (−11.8)
2dd-bi	−8.2 (−13.2)
2(d+H)₂	0.7 (4.8)

^aEnergy values in parentheses are relative to the parent compound **1**, assuming that both generated monomeric species **2** react with two Gly-Gly ligands.

one or two substrate molecules may coexist in equilibrium. Among all calculated complexes the lowest energy structure, **2a0d** ($\Delta G_{\text{aq}}^{\text{compl}} = -9.1 \text{ kcal mol}^{-1}$), contains two Gly-Gly molecules, one coordinated through the –C=O and –NH₂ groups and the other through the –COO[−] group (Figure 5). Energy contributions to the aqueous free energy of all complex species can be found in Table S3 of the Supporting Information.

On the basis of the results thus obtained, the species **2a0d** and **2a-H** may be considered as the most probable candidates responsible for the hydrolytic activity of **1**. In both complexes the peptide bond of the bidentate-bound Gly-Gly ligand is activated toward nucleophilic attack through polarization of the –C=O bond by the Zr(IV) ion. On the one hand **2a0d** reveals the highest stability, while on the other hand **2a-H** contains an intramolecular –OH nucleophile, which is a good premise for the high hydrolytic ability of this species. These two complexes were used for the mechanistic investigations in the next section.

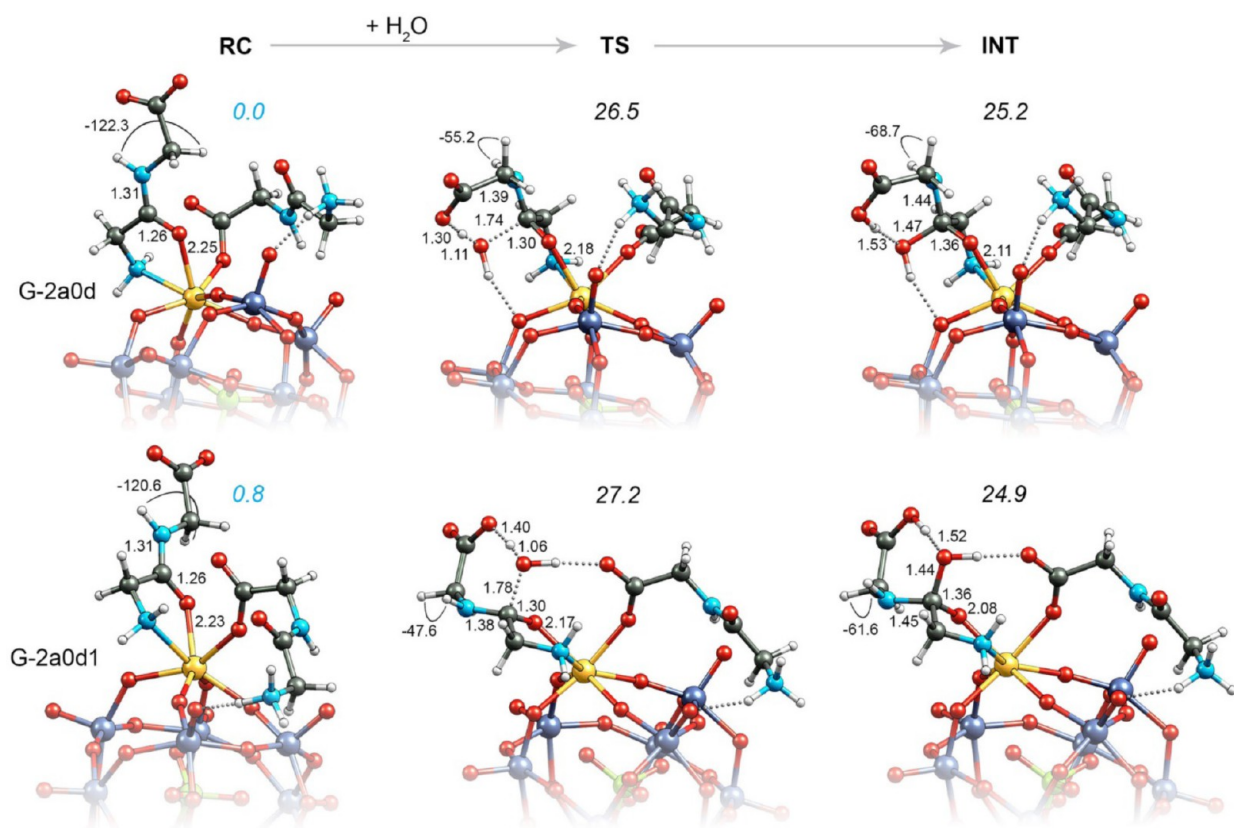


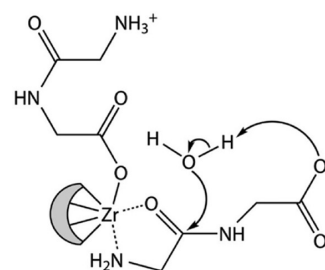
Figure 5. Optimized RC, TS, and INT structures involved in the rate-determining step of Gly-Gly hydrolysis via the **2a0d** path. Bond lengths, dihedral angles, and relative free energies (in *italics*) are given in Å, deg, and kcal mol⁻¹, respectively. The energy values colored in cyan indicate the relative stability of the RC complexes, while the TS and INT energies (in black) are calculated with respect to the energies of the corresponding starting RC conformations and a free H₂O molecule. All energy values were obtained with the M06 functional.

Mechanism of Gly-Gly Hydrolysis Catalyzed by the Monomeric Compound **2.** Free energy surfaces of the possible mechanistic scenarios were probed by means of M06-2X, M06, and BMK density functionals. The results obtained with the three functionals are in good qualitative agreement. Therefore, unless otherwise noted, only the M06 energy values will be discussed below.

In a recent theoretical investigation on the mechanism of Gly-Gly hydrolysis catalyzed by a dimeric tetrazirconium(IV) Wells–Dowson POM,²³ we have shown that in the hydrolytically active complex the substrate is bidentate-coordinated to one Zr(IV) center, by analogy with **2a0d**, and that nucleophilic attack by a water molecule on the amide C atom is assisted by the ligand –COO⁻ group. This water addition step was found to be the bottleneck of the whole process of hydrolysis.²³ A similar mechanism could be proposed for the **2a0d** species, while in the **2a-H** species the intramolecular Zr–OH attack dominates over the –COO⁻-assisted hydrolysis. There are two ligand –COO⁻ groups in the **2a0d** complex which potentially could act as a general base: one is Zr-bound, while the other is free. Since the first is a weaker proton acceptor than the latter, the hydrolytic mechanism here most likely involves nucleophilic attack by a solvent water molecule with proton abstraction by the free –COO⁻ group of Gly-Gly, as shown in **Scheme 2**. This reaction path will be further referred to as the “**2a0d** path”.

Because water addition to the amide C atom is expected to be the rate-determining step along the **2a0d** path, our efforts were mainly focused on modeling this reaction step. The **2a0d**

Scheme 2. Principal Mechanism of Nucleophilic Attack on the Amide Carbon Atom of Gly-Gly in the **2a0d** Complex



species itself encompasses several conformations with similar stabilities corresponding to different mutual orientations of the two Gly-Gly ligands and the POM, and the preferential stability order of these conformations changes with the applied functional. Moreover, different reactant complexes (RC) are connected to different TSs for nucleophilic attack on the PES. To deal with this complex situation, we have considered several initial conformations, and their associated TSs, instead of just the one RC conformation with the lowest energy, as predicted by a certain functional. The number of conformations was limited by selecting only those whose relative stabilities, calculated with the M06-2X functional, lie within 2 kcal mol⁻¹. In this way the lowest energy **2a0d** conformations predicted by the three functionals are included and examined. Two RC conformations, **G-2a0d** (as also predicted by B3LYP in the binding study) and **G-2a0d1**, were selected and are depicted in **Figure 5**. In the lowest energy TS connected to **G-**

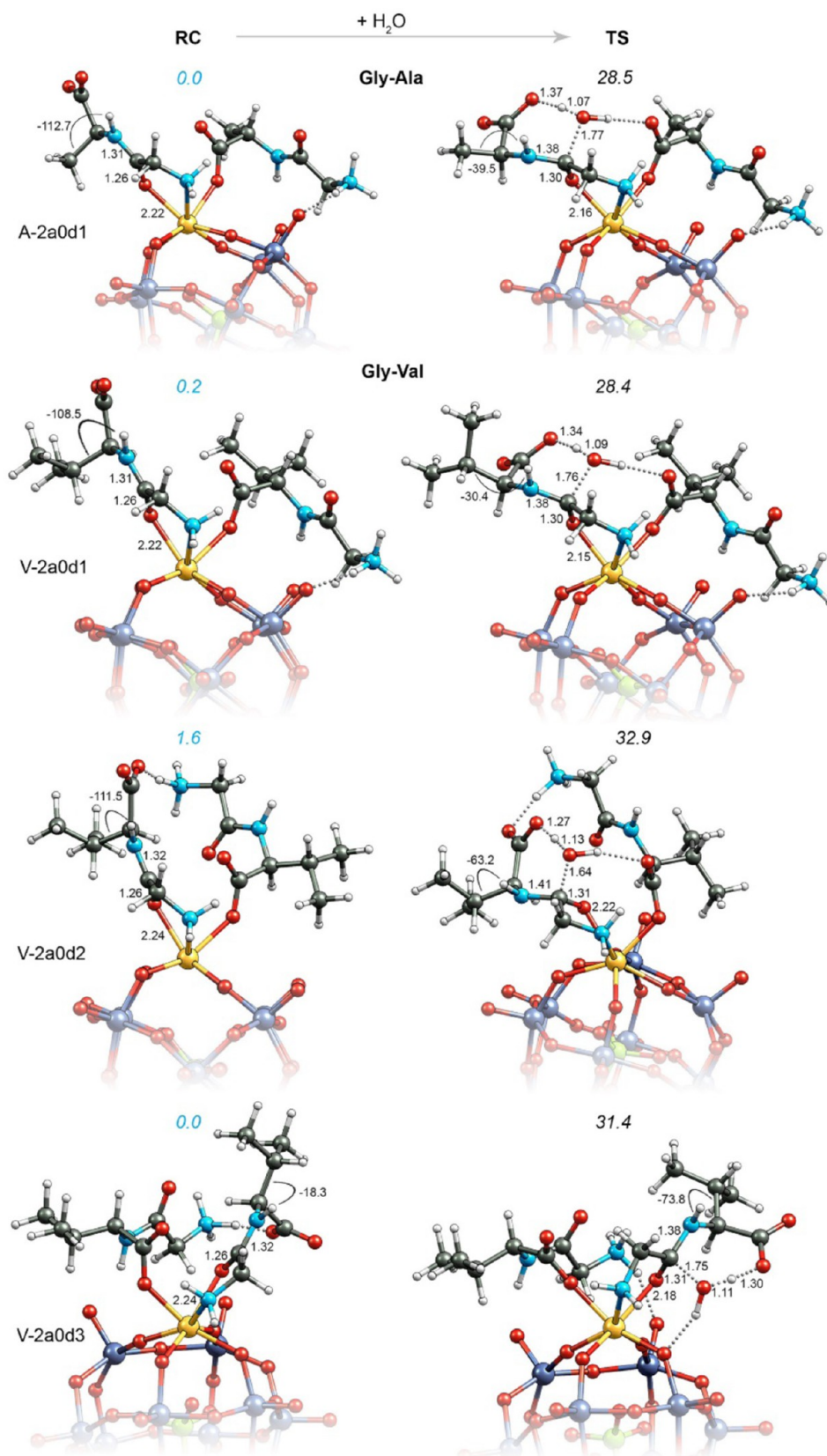


Figure 6. Optimized RC and TS structures involved in the rate-limiting hydrolytic step of Gly-Ala and Gly-Val when bound to **2** through the **2a0d** binding mode. Bond lengths, dihedral angles, and relative free energies (in *italics*) are given in Å, deg, and kcal mol⁻¹, respectively. The energy values colored in cyan indicate the relative stability of the RC complexes, while the TS energies (in black) are calculated with respect to the energies of the corresponding starting RC conformation and a free H₂O molecule. All energy values were obtained with the M06 functional.

2a0d on the PES, the attacking water molecule is H-bonded to a bridging oxygen atom of the POM skeleton while the free ligand $-\text{COO}^-$ group abstracts a H_2O proton and the nascent OH nucleophile attacks the amide carbon atom. This process requires $26.5 \text{ kcal mol}^{-1}$. The TS relaxes to the unstable intermediate INT with an energy lowering of only $1.3 \text{ kcal mol}^{-1}$ (Figure 5). On the other hand, in the TS structure connected to **G-2a0d1**, the attacking water molecule is H-bonded to a $\text{Zr}-\text{O}-\text{C}=\text{O}$ oxygen atom of the neighboring Gly-Gly ligand. The calculated energy barrier associated with this process is $27.2 \text{ kcal mol}^{-1}$, and a similar TS \rightarrow INT energy lowering of $2.3 \text{ kcal mol}^{-1}$ was also found. Hence, on average the **2a0d** path of hydrolysis requires an activation energy of around 27 kcal mol^{-1} . It should be noted that the three functionals used here tend to underestimate the INT stability,²³ which may explain the small TS-INT energy difference. Additional energy data are provided in Table S4 of the Supporting Information.

The hydrolytic mechanism originating from the **2a-H** species, further referred to as the **2a-H** path, was also thoroughly examined. The results are presented and discussed in the Gly-Gly hydrolysis via **2a-H** path section (Figures S8–S10 and Tables S5 and S6) of the Supporting Information. As expected, intramolecular OH attack on the amide C atom with formation of a tetrahedral intermediate proceeds with a low energy barrier, estimated as $18.8 \text{ kcal mol}^{-1}$. The rate-determining step along this path, however, is the last reaction step corresponding to a water-mediated proton transfer from the $-\text{OH}$ group to the amide nitrogen atom with a subsequent substrate decomposition. This process requires $23.8 \text{ kcal mol}^{-1}$, which is lower than the activation energy associated with the **2a0d** path by about 3 kcal mol^{-1} .

The experimental ΔH^\ddagger and ΔS^\ddagger values for Gly-Gly hydrolysis in the presence of **1** were previously estimated to be $20.9 \text{ kcal mol}^{-1}$ and $-29.4 \text{ cal mol}^{-1} \text{ K}^{-1}$, giving $\Delta G^\ddagger(25^\circ\text{C}) = 28.3 \text{ kcal mol}^{-1}$.^{10b} The predicted activation energy for the **2a0d** path (27 kcal mol^{-1}) is in better agreement with the experiment than that for the **2a-H** path, thus suggesting the **2a0d** species/mechanism to be responsible for the observed peptide hydrolysis. Interestingly, the rate of Gly-Gly hydrolysis in the presence of the dimeric tetrazirconium(IV) Wells–Dawson POM, $k_{\text{obs}} = 2.97 \times 10^{-7} \text{ s}^{-1}$, is very similar to that determined here ($4.44 \times 10^{-7} \text{ s}^{-1}$).²³ This POM, however, does not contain a $\text{Zr}-\text{OH}$ function(s) and, in contrast to the case for **1**, it is stable over a broad range of experimental conditions.²³ In addition, the changes in the rate constants within the Gly-X series of dipeptides observed with the two catalysts follow the same trend. These findings strongly suggest that the mechanisms of Gly-X peptide bond hydrolysis catalyzed by the two POMs are rather similar, pointing out that the **2a0d** path (which is analogous to that proposed for the Zr_4 -POM) is indeed the most likely mechanism of hydrolysis.

The activation energy difference between **2a0d** and **2a-H** paths ($1\text{--}3 \text{ kcal mol}^{-1}$ with all three functionals; see Tables S4 and S6 of the Supporting Information) implies that hydrolysis should occur more quickly by a few orders of magnitude along the **2a-H** path. It has been shown that Zr(IV) complexes delivering an intramolecular OH nucleophile to the peptide bond are capable of hydrolyzing 90% of Gly-Gly within 20 h, at neutral pH and 60°C ,⁵¹ which is significantly faster than the reaction rates observed here (with half-lives of more than 2 weeks). Taking into account the calculated difference in the stabilities of the two complexes **2a-H** ($-4.5 \text{ kcal mol}^{-1}$, Table

2) and **2a0d** ($-9.1 \text{ kcal mol}^{-1}$, Table 3) and the possible existence of other species more stable than **2a-H** (e.g., **2d+H**, **2dc+H**, and **2dd-bi**), it seems evident that the equilibrium concentration of **2a-H** in the reaction mixture is probably too low to influence the hydrolysis rate.

Effect of the α -Substituent on the POM-Catalyzed Hydrolysis of Dipeptides with Aliphatic Side Chains. Due to the similarity of the Gly-X substrates and their rates of hydrolysis, the findings obtained for Gly-Gly should also be valid for the rest of dipeptides in the series. To trace the effects of the aliphatic side chains on the reaction kinetics, the hydrolysis of Gly-Ala and Gly-Val via the **2a0d** path was examined. Unfortunately, the comparatively higher side chain flexibility of Gly-Leu, Gly-Ile, and Gly-Phe, in combination with the variety of different mutual orientations of the two ligands and the POM in the complexes, requires an extensive DFT conformational search which substantially increases the computational cost. Therefore, substrate-catalyst complexes and TSs with these three ligands were not modeled. It should be mentioned that the differences among the rate constants in the Gly-X series are small, corresponding to activation free energy differences smaller than 1 kcal mol^{-1} . This is below the accuracy of the present computational chemistry approaches. However, since Gly-Gly, Gly-Ala, and Gly-Val differ only in the size of the aliphatic residue and the nature of both RCs and TSs is the same for the three ligands, the predicted trends should be reliable due to error cancellation. By analogy with Gly-Gly, only RC conformations with relative stabilities less than 2 kcal mol^{-1} were considered. For the Gly-Ala complex of **2** the three density functionals agree that **A-2a0d1** (Figure 6), which is analogous to **G-2a0d1**, is the most stable conformation. The corresponding TS is also analogous to that located for Gly-Gly, but the free energy barrier now amounts to $28.5 \text{ kcal mol}^{-1}$. In the case of Gly-Val three reactant complexes were selected: **V-2a0d1**, **V-2a0d2**, and **V-2a0d3** (Figure 6). Complex **V-2a0d1** is analogous to **G-2a0d1** and **A-2a0d1**, while in the complexes **V-2a0d2** and **V-2a0d3** a H bond is formed between the $-\text{NH}_3^+$ and the $-\text{COO}^-$ groups of the two ligands. The calculated free energy barriers for nucleophilic addition of a water molecule in the **V-2a0d1**, **V-2a0d2**, and **V-2a0d3** forms are 28.4 , 32.9 , and $31.4 \text{ kcal mol}^{-1}$, respectively (or 31 kcal mol^{-1} on average). Thus, on average the calculations predict an increase of the activation energy (decrease in the rate constants) in the order Gly-Gly < Gly-Ala < Gly-Val, which is in full agreement with experiment. Activation energies calculated with the M06-2X and BMK functionals are collected in Table S7 of the Supporting Information.

A closer look at the TS structures in Figures 5 and 6 reveals that in all cases the aliphatic side chains do not hinder the attacking nucleophile. Indeed, the distance between the H_2O oxygen and the closest C atom of the side chain is always greater than 4.4 \AA . Thus, the experimentally observed reaction rate decrease in the Gly-X series cannot be explained in terms of steric hindrance of the attacking nucleophile. Interestingly, we found that the decrease in the hydrolysis rate in the presence and in the absence of **1** follows the same trend. The uncatalyzed reactions are, however, too slow under these experimental conditions to determine the corresponding rate constants (Table 1). To describe the uncatalyzed hydrolysis in terms of activation energies, the water addition step to the free Gly-Gly, Gly-Ala, and Gly-Val dipeptides was also modeled (the mechanism of the uncatalyzed Gly-Gly hydrolysis was previously reported by us²³). In line with experiment the

calculated activation free energies of Gly-Gly, Gly-Ala, and Gly-Val are 32.0, 32.6, and 34.1 kcal mol⁻¹, respectively. Relevant structures and energy data can be found in Figure S11 and Table S8 of the Supporting Information. These results suggest that the trend in the observed rate constants of the POM-catalyzed reactions might be related to an inherent property of the substrates. To check whether the α substituent can influence the electron density distribution of the peptide bond and potentially alter the susceptibility of the amide carbon toward nucleophilic attack, a number of molecular descriptors, e.g. NBO analysis, Hirshfeld charges, and atomic electrostatic potential, were computed for all dipeptides in the Gly-X series. The results showed insignificant changes in the peptide bond properties when changing the aliphatic side chain; see Table S9 of the Supporting Information. A reasonable explanation, however, can be found on the basis of the substrate conformational changes in the complexes of Gly-Gly, Gly-Ala, and Gly-Val upon activation. As can be seen in Figures 5 and 6, the dihedral angle H-N-C _{α} -H _{α} (where H _{α} is the α -hydrogen atom being substituted in the L enantiomers of the corresponding dipeptides) decreases, in absolute values, from -122 to -105° in the RCs to -60 to -30° in the TS structures. Substitution of H _{α} in Gly-Gly with a bulky aliphatic substituent is expected to increase the steric hindrance between the amide hydrogen and the α substituent in the rate-limiting transition state, thus increasing the activation energy for hydrolysis. To check this assumption, the energy change of the free Gly-Gly, Gly-Ala, Gly-Val, Gly-Leu, Gly-Ile and Gly-Phe dipeptides as a function of the H-N-C-C _{α} (or H _{α}) angle was examined by means of the M06-2X functional. The results are plotted in Figure 7. As can be seen in Figure 7, within the range -60 to -30° (TS range) the rotational barrier increases in the order Gly-Gly < Gly-Ala < Gly-Phe < Gly-Val < Gly-Ile, which is in perfect agreement with the experimentally observed

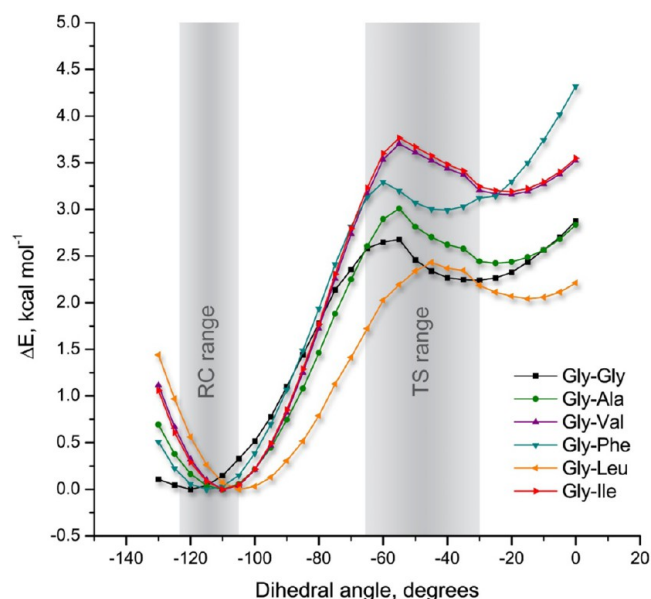


Figure 7. Energy profile of the H-N-C-C _{α} (or H _{α}) dihedral angle rotation in Gly-Gly, Gly-Ala, Gly-Val, Gly-Leu, Gly-Ile, and Gly-Phe dipeptides obtained with relaxed PES scans at the CPCM-M06-2X/6-311+G(2df,2p) level of theory. The ranges of calculated dihedral angles for both RCs and TSs of the Gly-Gly, Gly-Ala, and Gly-Val complexes with **2** (**2a0d** binding mode) are indicated as “RC range” and “TS range”, respectively.

decrease in the rate constants of the POM-catalyzed reactions. The only disagreement with the experimental trend was found for Gly-Leu, with a rotational energy barrier lower than that of Gly-Gly. Obviously, other factors such as weak intramolecular ligand–ligand and/or ligand–POM interactions, which could additionally stabilize/destabilize either the initial RC or the activated TS states, also contribute to the barrier height.

CONCLUSIONS

A detailed examination of the effect of the bulkiness of the amino acid side chain on the hydrolysis rate of a series of dipeptides with the Gly-X sequence in the presence of a dimeric Zr(IV)-substituted Keggin POM was performed by means of a combined theoretical–experimental approach. The observed rate of peptide bond hydrolysis was found to decrease with an increase in the side chain bulkiness in the order Gly-Gly > Gly-Ala > Gly-Phe > Gly-Leu \approx Gly-Val > Gly-Ile. Experimental data, reported previously by us,^{10b} evidenced that a Gly-Gly–catalyst complex involving coordination of both amide -C=O and terminal -NH₂ groups to the Zr(IV) center of the POM is formed prior to hydrolysis. DFT calculations, presented here, revealed that coordination of the substrate to the starting compound **1** is thermodynamically not favored and that Gly-Gly instead binds to the monomeric POM derivative **2**, which is also present in equilibrium with **1**. The formation free energy associated with the experimentally suggested coordination mode of Gly-Gly to **1** is calculated to be rather endergonic: 11.9 kcal mol⁻¹ (at pD 6.4). In contrast, bidentate coordination through the -C=O and -NH₂ groups to **2** was predicted to be exergonic by -5.6 kcal mol⁻¹. The stability of this species is further increased upon binding of a second Gly-Gly ligand, through the terminal -COO⁻ group, as the net complexation free energy becomes -14.8 kcal mol⁻¹. The latter is considered as the major player in the peptide bond cleavage. The mechanism of hydrolysis involves nucleophilic attack by a solvent water molecule on the amide carbon atom of the bidentate-bound ligand. This process is assisted by the free -COO⁻ group of the same ligand, which acts as a general base to abstract a proton from the attacking water molecule. Since the uncatalyzed hydrolysis of Gly-X dipeptides is also assisted by the carboxylic group, the main catalytic role of the POM can be attributed to the electrophilic activation of the carbonyl moiety by the Zr(IV) ion. The alternative mechanism involving intramolecular nucleophilic attack by a Zr-OH group was ruled out because this mechanism implies hydrolysis rates significantly higher than those observed in this study.

The decrease of the hydrolysis rate with increase of the side chain bulkiness is mostly due to the increased ligand conformational strain in the rate-limiting transition state which elevates the reaction activation energy. This conformational strain is imposed by the steric hindrance between the amide hydrogen atom and the α substituent. It increases first upon substitution of H _{α} in Gly-Gly with an aliphatic α substituent and second with the β branching of the α substituent. This explanation should also be valid for the hydrolysis of Gly-X in the presence of a dimeric tetrazirconium(IV) Wells–Dawson POM, where the same trend in the rate constants was observed. This work demonstrates the power of a combined theoretical and experimental study to unravel the molecular origin of the catalytic activity of metal-substituted POMs toward organic transformations, especially since reactivity studies on these types of compounds are often

hampered by the rich solution chemistry of metal-substituted POMs.

■ ASSOCIATED CONTENT

Supporting Information

The Supporting Information is available free of charge on the ACS Publications website at DOI: 10.1021/acs.inorgchem.6b01461.

¹H NMR spectra, additional computational details, a discussion of Gly-Gly binding to **1**, energy contributions to the aqueous free energies of the Gly-Gly-POM complexes, a discussion of the **2a-H** path of hydrolysis, energy contributions to the relative free energies of the stationary points along the reaction paths calculated with the M06, M06-2X, and BMK functionals, and molecular structures of relevant species in Cartesian coordinates (PDF)

■ AUTHOR INFORMATION

Corresponding Author

*E-mail for T.T.M.: tzvetan.mihaylov@kuleuven.be.

Notes

The authors declare no competing financial interest.

■ ACKNOWLEDGMENTS

T.T.M. thanks the FWO Flanders for financial support under project G.0260.12. H.G.T.L. thanks the Vietnamese Government and KU Leuven for a doctoral fellowship. T.N.P.-V. thanks KU Leuven for financial support (OT/13/060). The computational resources and services used in this work were provided by the VSC (Flemish Supercomputer Center), funded by the Hercules Foundation and the Flemish Government—department EWI. The calculations were performed on the HPC cluster Tier-2 of KU Leuven.

■ REFERENCES

- (1) (a) Aebersold, R.; Mann, M. *Nature* **2003**, *422*, 198–207. (b) Gallop, M. A.; Barrett, R. W.; Dower, W. J.; Fodor, S. P. A.; Gordon, E. M. *J. Med. Chem.* **1994**, *37*, 1233–1251. (c) Cruz-Migoni, A.; Fuentes-Fernandez, N.; Rabbitts, T. H. *MedChemComm* **2013**, *4*, 1218–1221.
- (2) Radzicka, A.; Wolfenden, R. *J. Am. Chem. Soc.* **1996**, *118*, 6105–6109.
- (3) (a) Kozhevnikov, I. V. *Chem. Rev.* **1998**, *98*, 171–198. (b) Kozhevnikov, I. V. *Catalysis by Polyoxometalates*; Wiley: Chichester, U.K., 2002; Vol. 2. (c) Izarova, N. V.; Pope, M. T.; Kortz, U. *Angew. Chem., Int. Ed.* **2012**, *51*, 9492–9510. (d) Sartorel, A.; Bonchio, M.; Campagna, S.; Scandola, F. *Chem. Soc. Rev.* **2013**, *42*, 2262–2280.
- (4) (a) Muller, A.; Peters, F.; Pope, M. T.; Gatteschi, D. *Chem. Rev.* **1998**, *98*, 239–272. (b) Yamase, T. *Chem. Rev.* **1998**, *98*, 307–326.
- (5) (a) Stephan, H.; Kubeil, M.; Emmerling, F.; Muller, C. E. *Eur. J. Inorg. Chem.* **2013**, *2013*, 1585–1594. (b) Rhule, J. T.; Hill, C. L.; Judd, D. A. *Chem. Rev.* **1998**, *98*, 327–358.
- (6) Mizuno, N.; Misono, M. *Chem. Rev.* **1998**, *98*, 199–218.
- (7) Sadakane, M.; Steckhan, E. *Chem. Rev.* **1998**, *98*, 219–237.
- (8) (a) Lv, H.; Geletii, Y. V.; Zhao, C.; Vickers, J. W.; Zhu, G.; Luo, Z.; Song, J.; Lian, T.; Musaev, D. G.; Hill, C. L. *Chem. Soc. Rev.* **2012**, *41*, 7572–7589. (b) Sumliner, J. M.; Lv, H.; Fielden, J.; Geletii, Y. V.; Hill, C. L. *Eur. J. Inorg. Chem.* **2014**, *2014*, 635–644.
- (9) (a) Ishimoto, R.; Kamata, K.; Mizuno, N. *Angew. Chem., Int. Ed.* **2012**, *51*, 4662–4665. (b) Kamata, K.; Yonehara, K.; Sumida, Y.; Yamaguchi, K.; Hikichi, S.; Mizuno, N. *Science* **2003**, *300*, 964–966.
- (10) (a) Ly, H. G. T.; Absillis, G.; Bajpe, S. R.; Martens, J. A.; Parac-Vogt, T. N. *Eur. J. Inorg. Chem.* **2013**, *2013*, 4601–4611. (b) Ly, H. G. T.; Absillis, G.; Parac-Vogt, T. N. *Dalton Trans.* **2013**, *42*, 10929–10938. (c) Ly, H. G. T.; Absillis, G.; Janssens, R.; Proost, P.; Parac-Vogt, T. N. *Angew. Chem., Int. Ed.* **2015**, *54*, 7391–7394.
- (11) (a) Kato, C. N.; Negishi, S.; Yoshida, K.; Hayashi, K.; Nomiya, K. *Appl. Catal., A* **2005**, *292*, 97–104. (b) Kholdeeva, O. A.; Maksimovskaya, R. I. *J. Mol. Catal. A: Chem.* **2007**, *262*, 7–24. (c) Kholdeeva, O. A.; Maksimov, G. M.; Maksimovskaya, R. I.; Vanina, M. P.; Trubitsina, T. A.; Naumov, D. Y.; Kolesov, B. A.; Antonova, N. S.; Carbo, J. J.; Poblet, J. M. *Inorg. Chem.* **2006**, *45*, 7224–7234.
- (12) (a) Mizuno, N.; Yamaguchi, K.; Kamata, K. *Coord. Chem. Rev.* **2005**, *249*, 1944–1956. (b) Mizuno, N.; Kamata, K.; Yamaguchi, K. *Top. Catal.* **2010**, *53*, 876–893. (c) Kato, C. N.; Hayashi, K.; Negishi, S.; Nomiya, K. *J. Mol. Catal. A: Chem.* **2007**, *262*, 25–29. (d) Estrada, A. C.; Santos, I. C. M. S.; Simoes, M. M. Q.; Neves, M. G. P. M. S.; Cavaleiro, J. A. S.; Cavaleiro, A. M. V. *Appl. Catal., A* **2011**, *392*, 28–35.
- (13) Kikukawa, Y.; Yamaguchi, S.; Nakagawa, Y.; Uehara, K.; Uchida, S.; Yamaguchi, K.; Mizuno, N. *J. Am. Chem. Soc.* **2008**, *130*, 15872–15878.
- (14) Boglio, C.; Lemiere, G.; Hasenknopf, B.; Thorimbert, S.; Lacote, E.; Malacria, M. *Angew. Chem., Int. Ed.* **2006**, *45*, 3324–3327.
- (15) Sartorel, A.; Carraro, M.; Scorrano, G.; Bassil, B. S.; Dickman, M. H.; Keita, B.; Nadjo, L.; Kortz, U.; Bonchio, M. *Chem. - Eur. J.* **2009**, *15*, 7854–7858.
- (16) Yasuda, H.; He, L. N.; Sakakura, T.; Hu, C. W. *J. Catal.* **2005**, *233*, 119–122.
- (17) Zhao, S.; Huang, L.; Song, Y.-F. *Eur. J. Inorg. Chem.* **2013**, *2013*, 1659–1663.
- (18) Orlandi, M.; Argazzi, R.; Sartorel, A.; Carraro, M.; Scorrano, G.; Bonchio, M.; Scandola, F. *Chem. Commun.* **2010**, *46*, 3152–3154.
- (19) (a) Absillis, G.; Parac-Vogt, T. N. *Inorg. Chem.* **2012**, *51*, 9902–9910. (b) Vanhaecht, S.; Absillis, G.; Parac-Vogt, T. N. *Dalton Trans.* **2013**, *42*, 15437–15446. (c) Ly, H. G. T.; Absillis, G.; Parac-Vogt, T. N. *New J. Chem.* **2016**, *40*, 976–984.
- (20) (a) Ly, H. G. T.; Absillis, G.; Parac-Vogt, T. N. *Eur. J. Inorg. Chem.* **2015**, *2015*, 2206–2215. (b) Stroobants, K.; Absillis, G.; Shestakova, P. S.; Willem, R.; Parac-Vogt, T. N. *J. Cluster Sci.* **2014**, *25*, 855–866.
- (21) (a) Stroobants, K.; Moelants, E.; Ly, H. G. T.; Proost, P.; Bartik, K.; Parac-Vogt, T. N. *Chem. - Eur. J.* **2013**, *19*, 2848–2858. (b) Stroobants, K.; Goovaerts, V.; Absillis, G.; Bruylants, G.; Moelants, E.; Proost, P.; Parac-Vogt, T. N. *Chem. - Eur. J.* **2014**, *20*, 9567–9577. (c) Stroobants, K.; Absillis, G.; Moelants, E.; Proost, P.; Parac-Vogt, T. N. *Chem. - Eur. J.* **2014**, *20*, 3894–3897.
- (22) Luong, T. K. N.; Shestakova, P.; Mihaylov, T. T.; Absillis, G.; Pierloot, K.; Parac-Vogt, T. N. *Chem. - Eur. J.* **2015**, *21*, 4428–4439.
- (23) Ly, H. G. T.; Mihaylov, T.; Absillis, G.; Pierloot, K.; Parac-Vogt, T. N. *Inorg. Chem.* **2015**, *54*, 11477–11492.
- (24) (a) Kato, C. N.; Shinohara, A.; Hayashi, K.; Nomiya, K. *Inorg. Chem.* **2006**, *45*, 8108–8119. (b) Nomiya, K.; Saku, Y.; Yamada, S.; Takahashi, W.; Sekiya, H.; Shinohara, A.; Ishimaru, M.; Sakai, Y. *Dalton Trans.* **2009**, 5504–5511.
- (25) Glasoe, P. K.; Long, F. A. *J. Phys. Chem.* **1960**, *64*, 188–190.
- (26) Neese, F. *WIREs Comput. Mol. Sci.* **2012**, *2*, 73–78.
- (27) (a) Becke, A. D. *Phys. Rev. A: At., Mol., Opt. Phys.* **1988**, *38*, 3098–3100. (b) Perdew, J. P. *Phys. Rev. B: Condens. Matter Mater. Phys.* **1986**, *33*, 8822–8824.
- (28) Weigend, F.; Ahlrichs, R. *Phys. Chem. Chem. Phys.* **2005**, *7*, 3297–3305.
- (29) Andrae, D.; Haeussermann, U.; Dolg, M.; Stoll, H.; Preuss, H. *Theor. Chim. Acta* **1990**, *77*, 123–141.
- (30) Neese, F. *J. Comput. Chem.* **2003**, *24*, 1740–1747.
- (31) (a) Eichkorn, K.; Treutler, O.; Öhm, H.; Häser, M.; Ahlrichs, R. *Chem. Phys. Lett.* **1995**, *240*, 283–290. (b) Eichkorn, K.; Weigend, F.; Treutler, O.; Ahlrichs, R. *Theor. Chem. Acc.* **1997**, *97*, 119–124.
- (32) Weigend, F. *Phys. Chem. Chem. Phys.* **2006**, *8*, 1057–1065.
- (33) Klamt, A.; Schüürmann, G. *J. Chem. Soc., Perkin Trans. 2* **1993**, *5*, 799–805.

- (34) (a) Yan, L.; López, X.; Carbó, J.; Sniatynsky, R.; Duncan, D.; Poblet, J. *J. Am. Chem. Soc.* **2008**, *130*, 8223–8233. (b) Mal, S. S.; Tröppner, O.; Ivanović-Burmazović, I.; Burger, P. *Eur. J. Inorg. Chem.* **2013**, *2013*, 1960–1967. (c) López, X.; de Graaf, C.; Maestre, J. M.; Bénard, M.; Rohmer, M.-M.; Bo, C.; Poblet, J. M. *J. Chem. Theory Comput.* **2005**, *1*, 856–861. (d) López, X.; Fernández, J.; Romo, S.; Paul, J.; Kazansky, L.; Poblet, J. *J. Comput. Chem.* **2004**, *25*, 1542–1549. (e) Fernandez, J.; López, X.; Bo, C.; de Graaf, C.; Baerends, E.; Poblet, J. *J. Am. Chem. Soc.* **2007**, *129*, 12244–12253. (f) Fernández, J. A.; López, X.; Poblet, J. M. *J. Mol. Catal. A: Chem.* **2007**, *262*, 236–242.
- (35) (a) Becke, A. D. *J. Chem. Phys.* **1993**, *98*, 5648–5652. (b) Lee, C.; Yang, W.; Parr, R. G. *Phys. Rev. B: Condens. Matter Mater. Phys.* **1988**, *37*, 785–789. (c) Stephens, P. J.; Devlin, F. J.; Chabalowski, C. F.; Frish, M. J. *J. Phys. Chem.* **1994**, *98*, 11623–11627.
- (36) Neese, F.; Wennmohs, F.; Hansen, A.; Becker, U. *Chem. Phys.* **2009**, *356*, 98–109.
- (37) (a) Grimme, S.; Ehrlich, S.; Goerigk, L. *J. Comput. Chem.* **2011**, *32*, 1456–1465. (b) Grimme, S.; Antony, J.; Ehrlich, S.; Krieg, H. *J. Chem. Phys.* **2010**, *132*, 154104–19.
- (38) Frisch, M. J.; Trucks, G. W.; Schlegel, H. B.; Scuseria, G. E.; Robb, M. A.; Cheeseman, J. R.; Scalmani, G.; Barone, V.; Mennucci, B.; Petersson, G. A.; Nakatsuji, H.; Caricato, M.; Li, X.; Hratchian, H. P.; Izmaylov, A. F.; Bloino, J.; Zheng, G.; Sonnenberg, J. L.; Hada, M.; Ehara, M.; Toyota, K.; Fukuda, R.; Hasegawa, J.; Ishida, M.; Nakajima, T.; Honda, Y.; Kitao, O.; Nakai, H.; Vreven, T.; Montgomery, J. A., Jr.; Peralta, J. E.; Ogliaro, F.; Bearpark, M.; Heyd, J. J.; Brothers, E.; Kudin, K. N.; Staroverov, V. N.; Keith, T.; Kobayashi, R.; Normand, J.; Raghavachari, K.; Rendell, A.; Burant, J. C.; Iyengar, S. S.; Tomasi, J.; Cossi, M.; Rega, N.; Millam, J. M.; Klene, M.; Knox, J. E.; Cross, J. B.; Bakken, V.; Adamo, C.; Jaramillo, J.; Gomperts, R.; Stratmann, R. E.; Yazyev, O.; Austin, A. J.; Cammi, R.; Pomelli, C.; Ochterski, J. W.; Martin, R. L.; Morokuma, K.; Zakrzewski, V. G.; Voth, G. A.; Salvador, P.; Dannenberg, J. J.; Dapprich, S.; Daniels, A. D.; Farkas, O.; Foresman, J. B.; Ortiz, J. V.; Cioslowski, J.; Fox, D. J. *Gaussian 09, Revision D.01*; Gaussian, Inc., Wallingford, CT, 2013.
- (39) Zhao, Y.; Truhlar, D. G. *Theor. Chem. Acc.* **2008**, *120*, 215–241.
- (40) Hay, P. J.; Wadt, W. R. *J. Chem. Phys.* **1985**, *82*, 299–310.
- (41) (a) Barone, V.; Cossi, M. *J. Phys. Chem. A* **1998**, *102*, 1995–2001. (b) Cossi, M.; Rega, N.; Scalmani, G.; Barone, V. *J. Comput. Chem.* **2003**, *24*, 669–681.
- (42) Boese, A. D.; Martin, J. M. L. *J. Chem. Phys.* **2004**, *121*, 3405–16.
- (43) (a) Pliego, J. R., Jr.; Riveros, J. M. *J. Phys. Chem. A* **2001**, *105*, 7241–7247. (b) Bryantsev, V. S.; Diallo, M. S.; Goddard, W. A., III. *J. Phys. Chem. B* **2008**, *112*, 9709–9719.
- (44) Zamyatnin, A. A. *Prog. Biophys. Mol. Biol.* **1972**, *24*, 107–123.
- (45) Constantino, E.; Rimola, A.; Rodríguez-Santiago, L.; Sodupe, M. *New J. Chem.* **2005**, *29*, 1585–1593.
- (46) (a) Bassil, B. S.; Dickman, M. H.; Kortz, U. *Inorg. Chem.* **2006**, *45*, 2394–2396. (b) Fang, X.; Anderson, T. M.; Hill, C. L. *Angew. Chem., Int. Ed.* **2005**, *44*, 3540–3544. (c) Gaunt, A. J.; May, I.; Collison, D.; Helliwell, M. *Acta Crystallogr., Sect. C: Cryst. Struct. Commun.* **2003**, *59*, i65–i66. (d) Gaunt, A. J.; May, I.; Collison, D.; Holman, K. T.; Pope, M. T. *J. Mol. Struct.* **2003**, *656*, 101–106. (e) Villanneau, R.; Carabineiro, H.; Carrier, X.; Thouvenot, R.; Herson, P.; Lemos, F.; Ribeiro, F. R.; Che, M. *J. Phys. Chem. B* **2004**, *108*, 12465–12471. (f) Carabineiro, H.; Villanneau, R.; Carrier, X.; Herson, P.; Lemos, F.; Ramôa Ribeiro, F.; Proust, A.; Che, M. *Inorg. Chem.* **2006**, *45*, 1915–1923.
- (47) Jiménez-Lozano, P.; Carbó, J. J.; Chaumont, A.; Poblet, J. M.; Rodríguez-Forteza, A.; Wipff, G. *Inorg. Chem.* **2014**, *53*, 778–786.
- (48) Boglio, C.; Hasenknopf, B.; Lenoble, G.; Rémy, P.; Gouzerh, P.; Thorimbert, S.; Lacôte, E.; Malacria, M.; Thouvenot, R. *Chem. - Eur. J.* **2008**, *14*, 1532–1540.
- (49) Ho, J.; Coote, M. L. *Theor. Chem. Acc.* **2010**, *125*, 3–21.
- (50) Burgess, J. *Metal Ions in Solution*; Halsted Press (Wiley): New York, 1978.
- (51) (a) Kassai, M.; Ravi, R. G.; Shealy, S. J.; Grant, K. B. *Inorg. Chem.* **2004**, *43*, 6130–6132. (b) Kassai, M.; Grant, K. B. *Inorg. Chem. Commun.* **2008**, *11*, 521–525.